University of Groningen

Structures of an Isopenicillin N Converting Ntn-Hydrolase Reveal Different Catalytic Roles for the Active Site Residues of Precursor and Mature Enzyme

Bokhove, Marcel; Yoshida, Hiromi; Hensgens, Charles M. H.; van der Laan, Jan Metske; Sutherland, John D.; Dijkstra, Bauke W.

IMPORTANT NOTE: You are advised to consult the publisher's version (publisher's PDF) if you wish to cite from it. Please check the document version below.

Document Version
Publisher's PDF, also known as Version of record

[Link to publication in University of Groningen/UMCG research database](#)

Structures of an Isopenicillin N Converting Ntn-Hydrolase Reveal Different Catalytic Roles for the Active Site Residues of Precursor and Mature Enzyme

Marcel Bokhove,[1] Hiromi Yoshida,[1,5] Charles M.H. Hensgens,[1,4] Jan Metske van der Laan,[2] John D. Sutherland,[3] and Bauke W. Dijkstra[1,*]

[1]Laboratory of Biophysical Chemistry, University of Groningen, Nijenborgh 4, 9747 AG Groningen, Netherlands
[2]Department DSM Food Specialties/R&D/PBA 566-0180, DSM Food Specialties, P.O. Box 1, 2600 MA Delft, Netherlands
[3]Department of Chemistry, University of Manchester, Oxford Road, Manchester M13 9PL, UK
[4]Present address: Crucell Holland B.V., P.O. Box 2048, 2301 CA Leiden, Netherlands
[5]Present address: Life Science Research Center, Kagawa University, 1705-1, Ikenobe, Miki-cho, Kita-gun, Kagawa, 761-0793, Japan
*Correspondence: b.w.dijkstra@rug.nl
DOI 10.1016/j.str.2010.01.005

SUMMARY

Penicillium chrysogenum Acyl coenzyme A:isopenicillin N acyltransferase (AT) performs the last step in the biosynthesis of hydrophobic penicillins, exchanging the hydrophilic side chain of a precursor for various hydrophobic side chains. Like other N-terminal nucleophile hydrolases AT is produced as an inactive precursor that matures upon posttranslational cleavage. The structure of a Cys103Ala precursor mutant shows that maturation is autoproteolytic, initiated by Cys103 cleaving its preceding peptide bond. The crystal structure of the mature enzyme shows that after autoproteolysis residues 92–102 fold outwards, exposing a buried pocket. This pocket is structurally and chemically flexible and can accommodate substrates of different size and polarity. Modeling of a substrate-bound state indicates the residues important for catalysis. Comparison of the proposed autoproteolytic and substrate hydrolysis mechanisms shows that in both events the same catalytic residues are used, but that they perform different roles in catalysis.

INTRODUCTION

Penicillins and cephalosporins are an efficacious group of β-lactam antibiotics produced by fungi such as *Penicillium chrysogenum*, *Acremonium chrysogenum*, and *Streptomyces clavuligerus*. In *P. chrysogenum*, the last step in the biosynthesis of hydrophobic penicillins is catalyzed by Acyl coenzyme A:isopenicillin N transferase (AT), which exchanges the α-aminoadipic acid side chain of isopenicillin N (IPN) for a coenzyme A-activated phenylacetic acid side chain, resulting in the formation of penicillin G (Figure 1). AT can also exchange other acyl side chains, accepting a wide range of acyl-CoA derivatives, hydrophobic as well as hydrophilic ones. It even accepts various non-CoA thioesters as substrate. This property makes AT an interesting enzyme for application in the (semi)synthetic production of β-lactam antibiotics (Alvarez et al., 1987; Barends et al., 2004; Demain and Elander, 1999; Whiteman et al., 1990).

AT is produced as a 40 kDa single chain precursor enzyme, which is autocatalytically activated by posttranslational cleavage of the Gly102-Cys103 peptide bond, resulting in a heterodimeric mature protein with subunits of 11 and 29 kDa (Aplin et al., 1993a; Tobin et al., 1990). Site-directed mutagenesis revealed several amino acid residues to be crucial for this posttranslational cleavage and enzymatic activity (Tobin et al., 1994, 1995). In particular, mutants of Cys103, which becomes the N-terminal residue of the 29 kDa β chain upon cleavage, were devoid of AT activity and remained in the inactive, 40 kDa precursor form (Tobin et al., 1995).

The posttranslational activation of AT resembles that of penicillin G acylase (PGA). In mature PGA the N-terminal serine residue of the β subunit Ser264 is in the active site, where it functions as the nucleophile in catalysis (Duggleby et al., 1995). This finding made PGA the founding member of the N-terminal nucleophile hydrolase (Ntn-hydrolase) superfamily (Brannigan et al., 1995). However, the N-terminal nucleophile is not only important for the activity of the mature enzyme, it is also essential for the autocatalytic processing of the precursor, as shown by the structure of a slow processing mutant of this enzyme (Hewitt et al., 2000). In that latter structure, the side chain of Ser264 is in an appropriate position to attack the carbonyl carbon atom of the scissile 263–264 peptide bond.

In the various Ntn-hydrolases structurally characterized until now, the N-terminal nucleophile can be a Ser, Thr, or Cys residue. Yet, the folding patterns of the enzymes are basically the same, consisting of four layers of α helices and β sheets (αββα motif), and with equivalent stereochemistry at the active site (Brannigan et al., 1995; Murzin, 1996; Oinonen and Rouvinen, 2000). So far, seven different subfamilies have been distinguished (see the SCOP database at http://scop.mrc-lmb.cam.ac.uk/scop/; Andreeva et al., 2004; Murzin et al., 1995). However, AT does not show obvious amino acid sequence homology to these or other enzymes, and therefore we initiated crystal structure determinations of precursor and mature AT to obtain deeper insights into its structure and functioning. AT appears to be a small representative of the Ntn-hydrolase
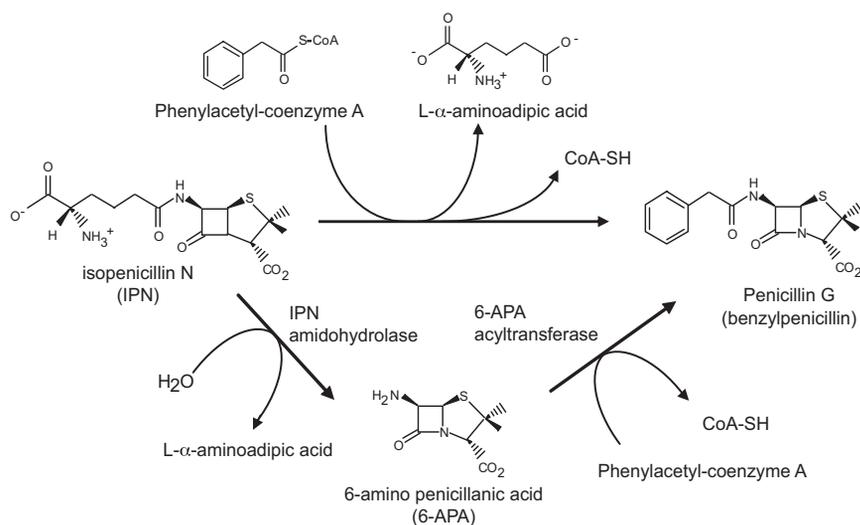
Figure 1. The Different Reactions Performed by AT, Including IPN Amidohydrolase- and 6-APA Acyltransferase Activity

superfamily, with which it shares the structural αββα motif. In the precursor mimic, residues 95 to 102 block access to the active site, but in mature AT these residues have departed from the active site, providing space for the binding of substrates. Analysis of the precursor structure and a tetrahedral reaction intermediate model pinpoint the important residues in autoproteolysis and catalysis. Interestingly, the same residues are involved in both processes, but they perform different roles in autoproteolysis and catalysis.

RESULTS AND DISCUSSION

Overall Structure of Mature and Precursor AT
Mature and Cys103Ala AT both crystallize in space group C2 with four molecules in the asymmetric unit (molecules A, B, C, and D), but with different crystal packing. Three of the four single chain Cys103Ala AT molecules are very similar, with rms differences ranging from 0.19 to 0.27 Å (for 354 Cα atoms). Molecule A shows larger rms differences of around 0.5 Å to the other molecules, mainly as a result of a different position of residues 39–50. These residues are part of a helix-turn-helix motif, which is folded away from the protein surface compared to the same region in chains B to D, suggesting that residues 37–50 have some plasticity.

In mature AT the Cα rms differences between three of the four molecules are also modest (0.28 to 0.40 Å for residues 1–97 and 103–355), again with molecule A deviating more (0.76 to 0.98 Å) from the other three AT molecules. These differences are again mainly caused by the region of residues 37–50 and the adjacent residues 90–102. As expected, the mature protein consists of two chains, the α subunit (residues 1–102) and the β subunit (residues 103–357) ([Aplin et al., 1993b](#)). While Cys103, which is the N terminus of the β chain, is well defined in all four molecules, the C-terminal residues of the α chain are flexible or disordered and are not visible in the electron density maps (undefined residues: molecule A, 102; molecule B, 99–102; molecule C, 98–102; molecule D, 99–102).

AT Is a Small Ntn-Hydrolase
Precursor and mature AT show the typical four-layered αββα fold (two β sheets sandwiched between two layers of α helices)

([Figures 2](#)A and 2B) that characterizes the Ntn-hydrolase superfamily ([Brannigan et al., 1995; Murzin, 1996; Oinonen and Rouvinen, 2000](#)). The SCOP database distinguishes seven Ntn-hydrolases. AT belongs to the subfamily with a cysteine as the N-terminal nucleophile. Indeed, a DALI search ([Holm and Sander, 1995](#)) shows that the β subunit of mature AT is most similar to Cys subfamily members penicillin V acylase (PVA; Z score 19.2, 10% sequence identity), the 66.3 kDa lysosomal mouse protein (Z score 19.8, 11% sequence identity), and the β subunits of the Ser subfamily members cephalosporin acylase (CA; Z score 25.1) and PGA (Z score 17.3). AT has also ~10% sequence identity to these latter enzymes. The α subunit of mature AT has much less similarity to the available protein structures, with highest Z scores of ~7.0 with the α subunits of PGA and CA.

Superposition of AT with PGA and CA reveals that AT lacks the structural extensions found in the other two family members. Its central stacked antiparallel β sheet is less extensive than in PGA and CA and the helices in the α domain are much shorter and lack the structural protrusions seen in PGA and CA. In addition, the β subunit of AT lacks the typical seven-stranded β barrel on the "B knob" ([Kim et al., 2000](#)) as well as the large α-helical bundle on the "A knob." Only short loops are present to connect the secondary structure elements that build up the αββα fold. The absence of the A and B knobs makes AT much less "chalice shaped" and far more compact than PGA and CA, giving it a small Ntn-hydrolase fold structure.

Comparison of the Structures of Precursor and Mature AT
Like other Ntn-hydrolases, AT is synthesized as a precursor enzyme that is proteolytically cleaved to yield the active enzyme. Mutants of Cys103 are not cleaved and the Cys103Ala mutant protein is therefore considered a good model of precursor AT ([Hensgens et al., 2002; Tobin et al., 1995](#)). Its structure shows that the molecule consists of a single chain, with the peptide bond between residues 102 and 103 intact ([Figure 2](#)A). In mature AT, however, this peptide bond is cleaved, with a Cα-101 to Cα-103 distance of over 25 Å (residue 102 is not visible in the electron density maps). No density extends from the α-amino group of Cys103 ([Figure 2](#)C), confirming that Cys103 has become the N-terminal residue of the β chain.

A more detailed comparison of mature and Cys103Ala AT shows that the two molecules have very similar overall structures, with an rms positional difference of only 0.33 Å for 344 of the 355 Cα atoms of the A molecules. Only residues 38–39, 95–101, and 254 differ by more than 0.65 Å; residue 102 is not visible in the mature enzyme. The largest conformational differences occur for residues 92–102. In precursor AT these residues
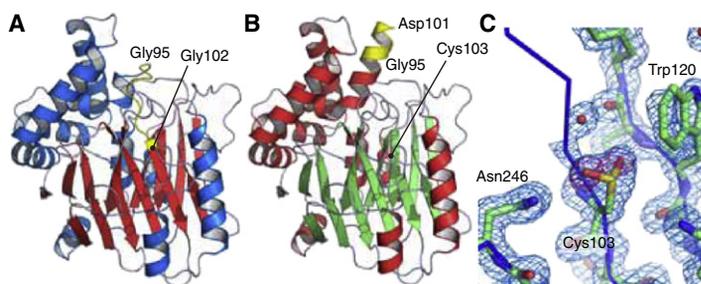
Figure 2. Comparison of the Precursor and Mature Structure of AT

(A) Structure of precursor AT with strands in red and helices in blue.
(B) Wild-type AT with strands in green and helices in red. In both (A) and (B), the precursor segment, residues 95–102, that folds out of the active site after maturation is indicated in yellow.
(C) Electron density of mature AT (blue, contoured at 1.2 σ), showing the oxidized side chain of Cys103 at the free N terminus. An mFo-DFc difference map (magenta, contoured at 5 σ) shows two strong peaks originating from the oxygen atoms covalently attached to the sulfur. For comparison, precursor AT is superposed in a blue ribbon representation.

form a loop that blocks the active site, but in mature AT they are part of an α helix that has moved out of the active site region. As a result, Cys103 has become accessible from the solvent after maturation, and the substrate binding cavity has opened up.

The Mechanism of Precursor Activation

The structure of Cys103Ala AT shows that the scissile peptide bond between residues 102 and 103 is not accessible to another enzyme or specific protease from the solvent, invalidating that the proteolytic activation of AT occurs intermolecularly. Instead, the precursor structure suggests that AT is activated by an intramolecular autocatalytic event, which has also been proposed for the cysteine-containing 66.3 kDa lysosomal mouse protein (Lakomek et al., 2009). A bound water molecule (Figure 3A, Wat1) is present that could act as the nucleophile in a one-step cleavage mechanism, but the absence of a catalytic base to activate the water molecule (see below) makes this mechanism unlikely. Furthermore, the Cys103 Sγ atom would place the water molecule in an unfavorable position to attack the carbonyl carbon of the scissile bond. Therefore, an intramolecular attack by the Cys103 side chain seems more likely. Indeed, replacing Ala103 by a cysteine in the Cys103Ala AT structure brings the Sγ atom near the carbonyl carbon atom of the Gly102-Cys103 scissile peptide bond (Figure 3A). The tight packing of the residues around the Cys103 side chain in the β sheet constrains the Cys103 side chain to a rotamer conformation with χ_1 close to 0°, placing the Sγ atom at ∼2.7 Å from the carbonyl carbon atom. This conformation allows a perpendicular intramolecular attack of Cys103 on the carbonyl carbon of the scissile peptide bond, resulting in a thioester intermediate via an N-S acyl rearrangement.

Such N-S or N-O acyl shifts have been proposed for other Ntn-hydrolases as well (Paulus, 2000). However, the nucleophile-activating mechanisms differ; a conserved water molecule that acts as a base has been proposed for CA and the proteasome subunits (Ditzel et al., 1998; Kim et al., 2002), while in glycosylasparaginase the residue preceding the N-terminal nucleophile is proposed to act as a general base (Xu et al., 1999). Neither mechanism can be applied to AT. First of all, AT lacks a highly coordinated water molecule that could act as a base, which is in agreement with the observation that a Cys103Ser mutant is incapable of self-cleavage (Tobin et al., 1995). Second, the only residue preceding Cys103 that could act as a base is Asp101; however, the Oδ atom of Asp101 is too far away from the C103 Sγ (4.7 Å), and Asp101 can be mutated without seriously affecting maturation (Tobin et al., 1995).

A nucleophile activation mechanism may not even be necessary for AT because of the greater nucleophilicity of a cysteine side chain compared to that of serine or threonine (Noren et al., 2000). With a pKa value of around 8.0 to 8.5 for a Cys side chain, the Cys103 thiol group may be deprotonated by the solvent. Indeed, a narrow water tunnel exists that may connect the side chain of residue 103 to the solvent. The ensuing thiolate ion can be stabilized by the backbone amide of Ala168 and the Nδ atom of Asn246, which are 3.2 Å and 3.4 Å away from the Cys103 Sγ, respectively. The Cys103 thiolate ion may then directly attack the carbonyl carbon atom of Gly102. A transient tetrahedral oxythiazolidine anion transition state is formed, which is stabilized by the backbone amide of Asp121. Next, a water molecule (Figure 3B, Wat2) can protonate the α-amino leaving group of Cys103, resulting in the collapse of the transition state into a thioester intermediate. Wat2 is located on the opposite side of the scissile peptide bond. It is held in place by hydrogen bonding and van der Waals interactions with the side chains of Asp121, Arg268, and Arg302. The Wat2 hydroxide ion is now able to attack the new thioester carbonyl carbon atom, again resulting in a tetrahedral transition state stabilized by the backbone amide of Asp121. Wat1 completes the reaction by protonating the cysteine Sγ atom and causing the collapse of the tetrahedral transition state into the free C- and N-terminal residues. Interestingly, except for Gly102 and Asp101, none of the amino acids in the precursor segment have strong interactions with the rest of the enzyme, indicating that it may easily fold away from the N-terminal nucleophile into the α helix found in the mature enzyme.

The Wat2 binding residues Arg268 and Asp121 form a hydrogen-bonding network with Asn246 and the carbonyl and amide backbone atoms of residue 103, which maintains the structural integrity of both the autocatalytic and catalytic site (see below). Arg268 is conserved in the AT homologs CA, PGA, and PVA, and mutation of this arginine in PGA gives rise to enzymes incapable of autocleavage (Alkema et al., 2002). No mutation studies to assess its (auto)catalytic importance have been reported for Asp121 or its equivalents in PGA or PVA.

Our data on the structure of precursor AT yet again provides a different model of Ntn-hydrolase zymogen activation compared to previous work (Ditzel et al., 1998; Kim et al., 2002; Xu et al., 1999). Our results suggest that the catalytic cysteine is self-activated for nucleophilic attack of the scissile peptide bond. The variations in activation mechanisms observed in the Ntn-hydrolase family are likely the result of the different nucleophiles present in the enzymes. Nevertheless, the intricate structural framework that underlies self-activation, such as the oxyanion hole and the nucleophile-stabilizing residues, is essentially conserved.
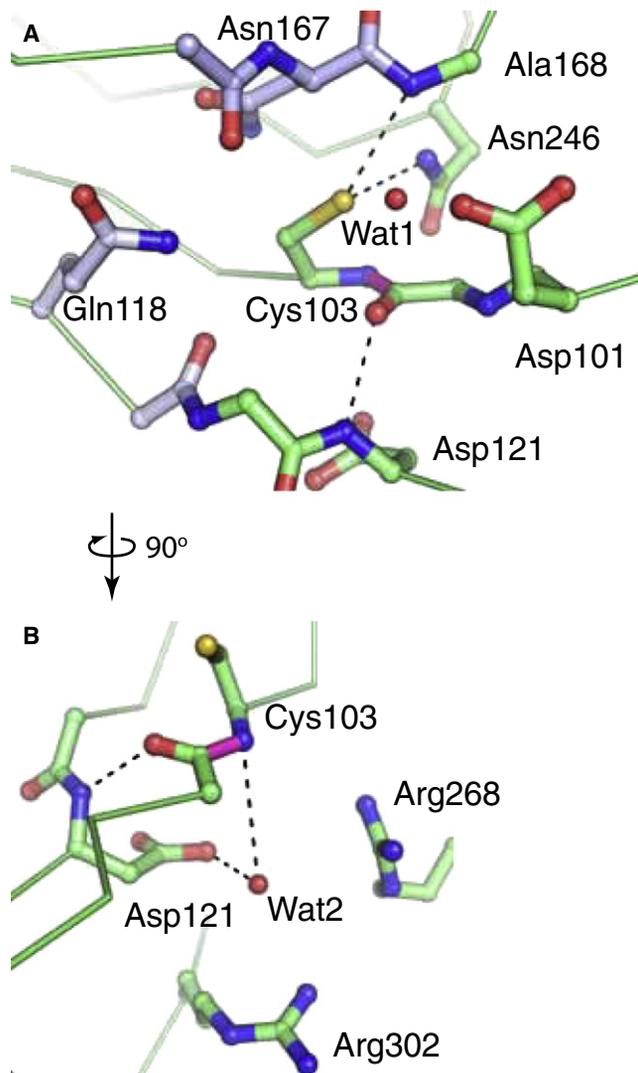
Figure 3. The Site of Autoproteolysis

(A) The autocatalytic environment of residue 103. The alanine residue in the crystal structure was replaced in silico by a cysteine. The scissile bond is indicated in magenta. The backbone atoms of residue 119 and 167 and the side chain of Gln118 (indicated in light blue) maintain the eclipsed conformation of Cys103 while the backbone amide of Ala168 and the Nδ of Asn246 stabilize the thiolate state. The backbone amide of Asp121 is involved in transition state stabilization.

(B) The site of Wat2 opposite to the Cys103 side chain. Wat2 is the putative proton donor that protonates the α-amino leaving group. The resulting OH⁻ nucleophile hydrolyzes the thioester intermediate.

Substrate Binding Site and Active Center of Wild-Type AT

The maturation of AT and the concomitant structural rearrangements of residues 38–39, 95–101, and 254 result in the formation of a large cavity with a narrow entrance. This cavity is already present in the precursor structure, but its entrance is blocked by residues 95–102 such that the substrate can not enter. The cavity is lined by hydrophilic and hydrophobic amino acids from both the α and β subunits, and with a volume of ~720 Å³ it is much larger than the substrate binding pockets found in CA and PGA.
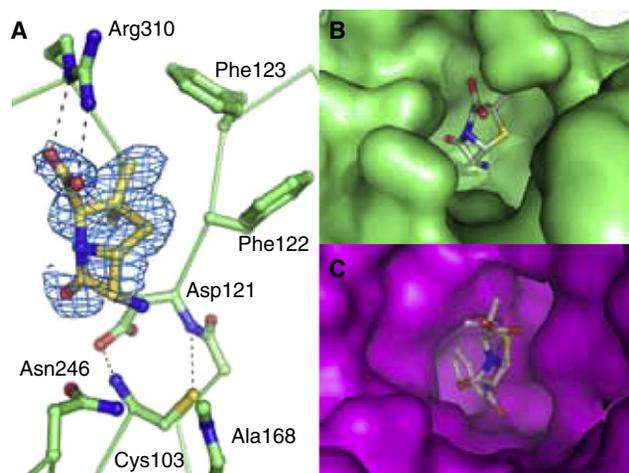

Figure 4. Substrate Binding Pocket of AT

(A) Binding of 6-APA in the substrate binding site with its composite omit electron density contoured at 1 σ. The important ligating and catalytic residues are indicated in ball and stick.

(B) Surface representation of AT with bound 6-APA.

(C) PGA with bound penicillin G (PDB entry 1FXV). AT has a more closed substrate binding site than PGA.

Co-crystallization of mature AT with the β-lactam core 6-aminopenicillanic acid (6-APA) revealed that 6-APA binds near Cys103. Its thiazole ring has Van der Waals interactions with Phe122 and Phe123, and its carboxylate group makes a salt bridge with Arg310 (Figure 4A). Compared to substrate/product binding in PGA and CA, 6-APA is buried much deeper in the AT active site cavity (Figures 4B and 4C), and its β-lactam group is much less solvent exposed and has more interactions with the enzyme. 495 Å² of solvent accessible surface area of the ligand is buried upon binding of 6-APA by AT, compared to ~375 Å² for the β-lactam nucleus buried in CA and PGA [1JVZ (Kim and Hol, 2001) and 1GM7 (McVey et al., 2001)].

To pinpoint catalytically important residues we attempted to model the substrate IPN in the active site of AT. This was not successful when starting from the observed 6-APA position because the α-aminoadipic acid side chain clashed with Leu262 and Arg302, which form part of the wall of the substrate binding site. Instead, based on the binding and coordination of penicillin G and PMSF in PGA [PDB entries 1FXV (Alkema et al., 2000) and 1PNM (Duggleby et al., 1995), respectively], we could model the tetrahedral reaction intermediate of IPN that results from a nucleophilic attack by the Cys103 Sγ on the carbonyl carbon of the substrate scissile bond (Figure 5A). The tetrahedral intermediate resembles the transition state, which is the chemical species actually recognized by the enzyme (Hermann et al., 2007). In the model, the α-aminoadipic acid part of IPN points into the substrate binding cavity, similar to the side chains of penicillin and glutaryl-7-aminocephalosporanic acid in PGA and CA, while the 6-APA part sits on top, closing off the cavity (Figure 5B). Several conformational rearrangements are required to allow IPN binding. Most notably, Trp120 at the bottom of the binding site must adapt its rotamer conformation to make room for the α-aminoadipic acid side chain. Lys154 and Gln118 may also adjust their side chain conformations to
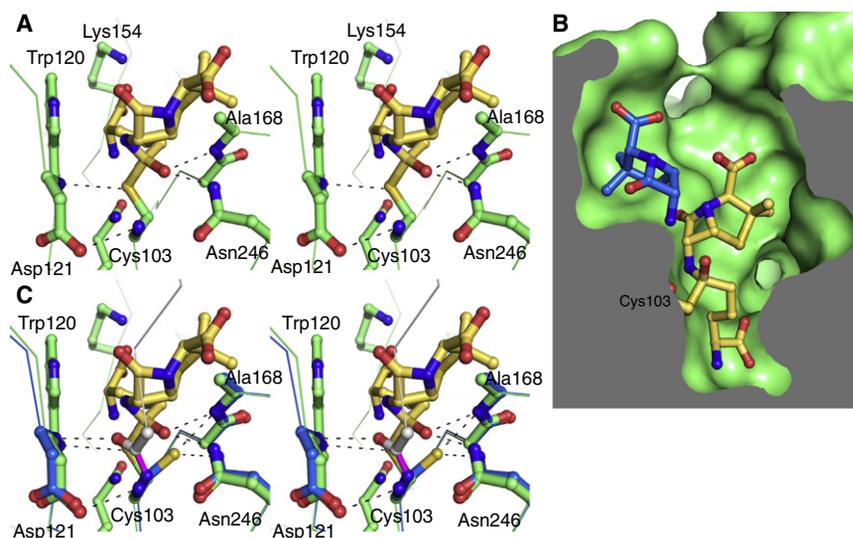
Figure 5. Comparison of the Precursor, Tetrahedral Intermediate Model, and 6-APA-Bound AT

(A) Modeled AT-IPN tetrahedral intermediate, in which the IPN is indicated in yellow and AT in green.

(B) A surface slice indicating the different binding modes of 6-APA (blue) and IPN (yellow). The 6-APA moiety of IPN (center of the figure) prevents the side chain (bottom) from leaving the substrate binding site. Therefore, the IPN 6-APA moiety is proposed to relocate to the experimentally observed 6-APA binding site (blue).

(C) Superposition of precursor AT (blue) with the tetrahedral intermediate model of wild-type AT (green). The α chain in the precursor structure is indicated in white, the precursor scissile peptide bond is indicated in magenta, and the catalytic and substrate binding residues are labeled.

make hydrogen bonds with the carboxylate and the amino group of the α-aminoadipic acid.

The model of the tetrahedral intermediate shows that the backbone amide of Ala168 and the Nδ atom of Asn246 are at hydrogen-bonding distance (2.9 Å and 3.1 Å, respectively) from the carbonyl oxygen of the substrate scissile bond (Figure 5A). This suggests that these groups form the oxyanion hole that stabilizes the tetrahedral transition state. An oxyanion hole comprising a backbone amide and an Nδ atom of an asparagine is highly conserved among Ntn-hydrolases. Other examples are the Alaβ69 backbone amide and Asnβ241 in PGA (Alkema et al., 2000; Duggleby et al., 1995) and the Valβ70 amide and Asnβ244 in CA (Kim and Hol, 2001). Interestingly, the substrate scissile bond in the tetrahedral intermediate model is flipped with respect to the precursor scissile peptide bond, of which the carbonyl oxygen points to the backbone amide of Asp121, which is located on the opposite side (Figure 5C). This implies that there are fundamental differences between transition state stabilization in precursor and substrate. Interestingly, the substrate-bound structures of PGA, CA, and γ-glutamyl transpeptidase (PDB entries 1FXV, 1JVZ, and 2DBW) also show this flipped orientation of the scissile bond compared to the orientation in the precursor (1E3A, 1KEH, and 2E0W), indicating that this may be a general property of Ntn-hydrolases.
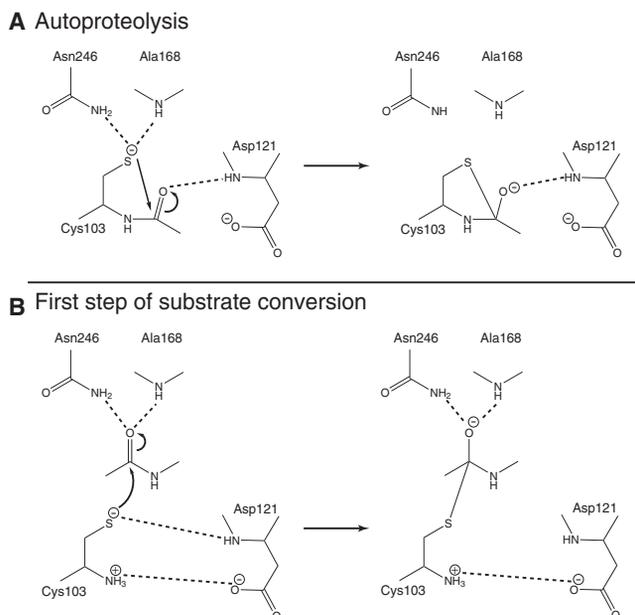
Our model indicates that Trp120 has to adapt its side chain conformation to permit substrate binding. The intrinsic conformational flexibility of the Trp120 side chain is apparent from its high B factors and the different conformations it takes up in the four AT molecules in the asymmetric unit. Other residues that line the substrate binding site, such as Lys154, Tyr166, and His182, also show high flexibility. Rotation of the Trp120 side chain expands the substrate binding site and exposes the deeply buried hydrophobic side chains of Leu130, Ile146, Leu314, and Phe315 and the hydrophilic side chains of Thr126 and Glu148. The chemically ambivalent character of the substrate binding pocket is in agreement with the observation that AT can accept both polar α-aminoadipyl and apolar phenylacetyl side chains. Furthermore, phenylacetyl-CoA is a competitive inhibitor for hydrolysis of IPN (containing an α-aminoadipoyl side chain), indi-

cating that both side chains bind in the same pocket (J.D.S., unpublished data). The structural as well as the chemical adaptability of the substrate binding site allows AT accommodating substrates of different size and polarity. This is unlike the rigid, hydrophilic or hydrophobic pocket found in CA and PGA, respectively, and seems to be a distinctive feature of AT that underlies its broad substrate specificity (Alvarez et al., 1993).

Our tetrahedral intermediate model shows a catalytic environment appropriate for the cleavage of the substrate peptide bond; however, in order to let the α-aminoadipic acid product leave the active site, 6-APA has to relocate since it blocks the exit path (Figure 5B). According to our 6-APA-bound structure 6-APA can be "stored" in a subpocket, creating room for the departure of α-aminoadipic acid. Subsequently, a new side chain can bind and be transferred to 6-APA from a donating group such as coenzyme A. An advantage of this temporary storage is that the transient acyl-enzyme intermediate, which is generated by transfer of a side chain from coenzyme A to Cys103, can be attacked by 6-APA before the acyl-enzyme is hydrolyzed by water. However, as of yet no data is available on the binding mode of coenzyme A-activated side chains.

Different Ways of Transition State Stabilization in Precursor and Mature AT

Comparison of the putative binding mode of a β-lactam substrate and the binding mode of the scissile bond of the precursor enzyme shows that the scissile bond in the substrate is rotated by 180° compared to the scissile bond in the precursor enzyme (Figure 5C). As a consequence, different ways of transition state stabilization are used in precursor and mature AT. In the precursor enzyme, the tetrahedral transition state is stabilized by the backbone amide of Asp121, while that of the substrate is stabilized by the Nδ of the Asn246 side chain and the backbone amide of Ala168, schematically represented in Figure 6. These latter residues lie on the opposite side of the substrate binding groove compared to Asp121. Because of this different orientation of the scissile bond, essential active site residues have different functions, depending on whether precursor or substrate is cleaved. While the Nδ atom of

A Autoproteolysis

Asn246   Ala168   Asn246   Ala168

Asp121   Asp121

Cys103   Cys103

B First step of substrate conversion

Asn246   Ala168   Asn246   Ala168

Asp121   Asp121

Cys103   Cys103

Figure 6. Comparison of the Formation of the Transition State in Autoproteolysis and Substrate Conversion
(A) In autoproteolysis the Nδ atoms of Asn246 and Ala168 backbone amide stabilize the reactive state of the nucleophilic Cys103 while the backbone amide of Asp121 stabilizes the negative charge on the oxythiazolidine anion transition state.
(B) Transition state formation during substrate conversion shows the opposite. Here the Nδ atoms of Asn246 and Ala168 backbone amide stabilize the substrate transition state while the backbone Oδ atom of Asp121 stabilizes the positively charged α-amino group and the backbone atom stabilizes the thiolate state of Cys103.

Asn246 forms part of the oxyanion hole during substrate cleavage, it stabilizes the thiolate state of Cys103 in the autoactivation reaction. Likewise, the backbone amide of Asp121 stabilizes the tetrahedral transition state during precursor activation, but its side chain Oδ atom and backbone amide stabilize the reactive state of Cys103 during substrate cleavage (Figure 5C). This dual role of the (auto)catalytic residues has also been noted in PGA (Hewitt et al., 2000). The substrate oxyanion hole groups stabilize the precursor Ser264 hydroxide prior to autoproteolysis, and the precursor oxyanion hole residues stabilize the N-terminal nucleophile during substrate hydrolysis. These observations indicate that Ntn-hydrolases are able to use the same functional groups to perform different roles in the cleavage of peptide bonds in substrate and precursor.

Application of AT in Antibiotic Synthesis

AT is of interest for the production of novel β-lactam antibiotics because it accepts a broad range of hydrophobic and hydrophilic side chains, such as CoA-activated phenylacetic and phenoxyacetic acid, as well as saturated and unsaturated C_5 to C_{10} fatty acids (Alvarez et al., 1993). Our results show that the structural and chemical adaptability of the side chain binding pocket are the main determinants of this broad specificity. Interestingly, AT is localized to the microbodies (or peroxisomes) (Müller et al., 1992) where β oxidation takes place. Intermediate

products of β oxidation are aliphatic CoA adducts, which supply AT with a wide variety of substrates (Luengo, 1995). The localization of AT to such an environment allows the enzyme to exercise its broad substrate specificity and produce an assortment of different penicillins, making the microbodies a high-throughput antibiotic production facility.

In contrast, with regard to the β-lactam nucleus, AT only accepts penicillins, and not cephalosporins (Alvarez et al., 1993). In the observed 6-APA binding site there is no room for the cephalosporin carboxylate, which lies in the plane of the cephem ring, whereas there is room for the axial substitution in penicillins (Figure 4B). This information can now be used to modify AT by site-directed mutagenesis to let it accept cephalosporins next to penicillins. However, to prevent such mutations from negatively affecting the maturation of AT, the permuted PGA construct of Flores et al. (2004) or the two-cistron construct of Tobin et al. (1995) seem to be suitable approaches for such research.

EXPERIMENTAL PROCEDURES

Overexpression and Purification
The mutant Cys103Ala AT precursor-like protein was prepared, purified, and crystallized as described previously (Hensgens et al., 2002). Mature wild-type AT was purified according to Yoshida et al. (2005).

Crystallization and Data Collection of Wild-Type and Cys103Ala AT
Wild-type AT was crystallized by hanging-drop vapor diffusion at room temperature. Aliquots of 2.0 μl of protein solution (9.03 mg/ml) were mixed with 2.0 μl of reservoir solution containing 25 mM acetate and 1.95 M phosphate (0.78 M NaH_2PO_4/1.17 M K_2HPO_4) (pH 6.9). Crystals appeared within 1 to 2 weeks. To characterize the substrate binding pocket of AT, mature wild-type AT was co-crystallized with 2.5 mM 6-APA (present in the precipitant solution). For data collection, crystals were flash-cooled in liquid nitrogen using mother liquor with 30% glycerol as cryoprotectant; data was collected at 100 K. Wild-type AT crystals showed diffraction to 1.64 Å, whereas the crystals of Cys103Ala AT diffracted to 1.85 Å. The crystals used for co-crystallization studies of AT with 6-APA diffracted to 2.0 Å. Data collection statistics are given in Table 1.

Structure Determination and Analysis
The diffraction data of wild-type AT was processed using DENZO and SCALEPACK (Otwinowski and Minor, 1997); XDS (Kabsch, 1993) was used for processing the data of Cys103Ala AT and a co-crystal of AT with 6-APA. Mature AT crystallized in space group $C2$ with cell dimensions $a = 198.7$, $b = 68.2$, $c = 147.0$ Å, and $β = 128.6°$. The Cys103Ala mutant AT crystallized in the same space group, but with cell dimensions $a = 230.9$, $b = 68.1$, $c = 150.9$ Å, and $β = 129.5°$.
The crystal structure of the Cys103Ala mutant was solved by selenomethionine MAD phasing at 3.5 Å resolution using 30 of the 32 Se sites (Schneider and Sheldrick, 2002). Phase extension to 1.85 Å resolution and automatic model building were done with ARP/wARP (Morris et al., 2003), and the obtained model was refined using REFMAC5 (Murshudov et al., 1997) to a final R factor of 16.9% at 1.85 Å resolution. The structure of mature AT was solved by molecular replacement with MOLREP (Vagin and Teplyakov, 1997), using the refined Cys103Ala mutant structure as starting model, and the structure was refined with REFMAC5 to a final R factor of 17.9% at 1.64 Å resolution. Electron density maps were interpreted using COOT (Emsley and Cowtan, 2004). The location of 6-APA in the 6-APA-AT complex structure was obtained from a difference electron density map, which was followed by refinement of the structure of the complex to a final R factor of 17.7% at 2.0 Å resolution. TLS refinement was used for all structures with one TLS group per molecule (Winn et al., 2003). Difference electron density maps revealed that the catalytic Cys103 was oxidized (Figure 2C). Structure validation was done with Molprobity (Davis et al., 2007), which indicated that in all mature AT structures and in

Table 1. Data Collection and Refinement Statistics

	preAT	wtAT	AT 6-APA
Beam line	ESRF ID14-1	ESRF ID14-1	DESY BW7A
Data collection			
Resolution (Å)	48.8−1.85 (1.95−1.85)	40.0−1.64 (1.68−1.64)	38.6−2.0 (2.11−2.00)
Space group	C2	C2	C2
Cell dimensions			
a, b, c (Å)	230.8, 68.1, 151.0	198.7, 68.2, 147.0	198.2, 68.4, 146.6
β (°)	129.5	128.6	128.8
R_{sym}[a] (%)	4.0 (21.2)	4.4 (35.1)	6.8 (38.2)
Wavelength (Å)	0.933	0.934	0.976
I/σ (I)	21.5 (5.4)	19.7 (2.1)	15.3 (3.8)
Completeness (%)	98.5 (98.6)	98.2 (99.2)	98.9 (98.3)
Redundancy	2.9 (2.7)	2.4 (1.9)	3.8 (3.7)
Refinement			
Resolution (Å)	48.8−1.85	34.1−1.64	33.8−2.00
No. reflections	145,184	175,358	97,033
R_{work}/R_{free}[b] (%)	16.9/19.3	17.9/20.7	17.7/20.2
Number of atoms			
Protein	11,388	11,367	11,231
Ligand/ion	73	51	72
Water	585	909	395
B factors			
Protein	29.7	26.8	29.1
Solvent	33.9	34.1	30.8
Rmsd			
Bond lengths (Å)	0.010	0.010	0.008
Bond angles (°)	1.113	1.255	1.162

Values in parentheses correspond to the highest resolution shell.

[a] $R_{sym} = \sum_{hkl}\sum_i |I_i(hkl) - <I(hkl)>|/\sum_{hkl}\sum_i I_i(hkl)$.

[b] $R = \sum |F_{obs}(hkl) - F_{calc}(hkl)|/\sum |F_{obs}(hkl)|$. R_{free} is the R value calculated for 5% of the data that were not included in the refinement.

all subunits the active site residue Lys154 lies outside the allowed region of the Ramachandran plot. Refinement statistics are summarized in Table 1.

The tetrahedral reaction intermediate was modeled as follows. First, IPN was placed in the substrate binding site by hand based on the orientation of penicillin G and PMSF in PGA (PDB entries 1FXV and 1PNM) (Alkema et al., 2000; Duggleby et al., 1995). Second, a covalent bond was introduced between the Sγ atom of Cys103 and the (tetrahedral) carbonyl carbon of the IPN scissile bond. After that, the geometry and nonbonding interactions of the protein side chains and the ligand were energy minimized using the "model_minimize" option in CNS_solve (Brünger, 2007); the protein backbone atoms were kept fixed.

ACCESSION NUMBERS

Coordinates and structure factors for precursor AT, wild-type mature AT, and AT in complex with 6-APA have been deposited at the RCSB Protein Data Bank under accession numbers 2X1C, 2X1D, and 2X1E, respectively.

ACKNOWLEDGMENTS

REFERENCES

Alkema, W.B., Hensgens, C.M.H., Kroezinga, E.H., de Vries, E., Floris, R., van der Laan, J.M., Dijkstra, B.W., and Janssen, D.B. (2000). Characterization of the beta-lactam binding site of penicillin acylase of *Escherichia coli* by structural and site-directed mutagenesis studies. Protein Eng. *13*, 857–863.

Alkema, W.B., Prins, A.K., de Vries, E., and Janssen, D.B. (2002). Role of alphaArg145 and betaArg263 in the active site of penicillin acylase of *Escherichia coli*. Biochem. J. *365*, 303–309.

Alvarez, E., Cantoral, J.M., Barredo, J.L., Diez, B., and Martin, J.F. (1987). Purification to homogeneity and characterization of acyl coenzyme A:6-aminopenicillanic acid acyltransferase of *Penicillium chrysogenum*. Antimicrob. Agents Chemother. *31*, 1675–1682.

Alvarez, E., Meesschaert, B., Montenegro, E., Gutierrez, S., Diez, B., Barredo, J.L., and Martin, J.F. (1993). The isopenicillin-N acyltransferase of *Penicillium chrysogenum* has isopenicillin-N amidohydrolase, 6-aminopenicillanic acid acyltransferase and penicillin amidase activities, all of which are encoded by the single penDE gene. Eur. J. Biochem. *215*, 323–332.

Andreeva, A., Howorth, D., Brenner, S.E., Hubbard, T.J., Chothia, C., and Murzin, A.G. (2004). SCOP database in 2004: refinements integrate structure and sequence family data. Nucleic Acids Res. *32*, D226–D229.

Aplin, R.T., Baldwin, J.E., Cole, S.C., Sutherland, J.D., and Tobin, M.B. (1993a). On the production of alpha, beta-heterodimeric acyl-coenzyme A: isopenicillin N-acyltransferase of *Penicillium chrysogenum*. Studies using a recombinant source. FEBS Lett. *319*, 166–170.

Aplin, R.T., Baldwin, J.E., Roach, P.L., Robinson, C.V., and Schofield, C.J. (1993b). Investigations into the post-translational modification and mechanism of isopenicillin N:acyl-CoA acyltransferase using electrospray mass spectrometry. Biochem. J. *294*, 357–363.

Barends, T.R.M., Yoshida, H., and Dijkstra, B.W. (2004). Three-dimensional structures of enzymes useful for beta-lactam antibiotic production. Curr. Opin. Biotechnol. *15*, 356–363.

Brannigan, J.A., Dodson, G., Duggleby, H.J., Moody, P.C., Smith, J.L., Tomchick, D.R., and Murzin, A.G. (1995). A protein catalytic framework with an N-terminal nucleophile is capable of self-activation. Nature *378*, 416–419.

Brünger, A.T. (2007). Version 1.2 of the Crystallography and NMR system. Nat. Protoc. *2*, 2728–2733.

Davis, I.W., Leaver-Fay, A., Chen, V.B., Block, J.N., Kapral, G.J., Wang, X., Murray, L.W., Arendall, W.B., 3rd, Snoeyink, J., Richardson, J.S., et al. (2007). MolProbity: all-atom contacts and structure validation for proteins and nucleic acids. Nucleic Acids Res. *35*, W375–W383.

Demain, A.L., and Elander, R.P. (1999). The beta-lactam antibiotics: past, present, and future. Antonie Van Leeuwenhoek *75*, 5–19.

Ditzel, L., Huber, R., Mann, K., Heinemeyer, W., Wolf, D.H., and Groll, M. (1998). Conformational constraints for protein self-cleavage in the proteasome. J. Mol. Biol. *279*, 1187–1191.

Duggleby, H.J., Tolley, S.P., Hill, C.P., Dodson, E.J., Dodson, G., and Moody, P.C. (1995). Penicillin acylase has a single-amino-acid catalytic centre. Nature *373*, 264–268.

Emsley, P., and Cowtan, K. (2004). Coot: model-building tools for molecular graphics. Acta Crystallogr. D Biol. Crystallogr. *60*, 2126–2132.

Flores, G., Soberon, X., and Osuna, J. (2004). Production of a fully functional, permuted single-chain penicillin G acylase. Protein Sci. *13*, 1677–1683.

Hensgens, C.M.H., Kroezinga, E.A., van Montfort, B.A., van der Laan, J.M., Sutherland, J.D., and Dijkstra, B.W. (2002). Purification, crystallization and preliminary X-ray diffraction of Cys103Ala acyl coenzyme A: isopenicillin N acyltransferase from *Penicillium chrysogenum*. Acta Crystallogr. D Biol. Crystallogr. *58*, 716–718.

Hermann, J.C., Marti-Arbona, R., Fedorov, A.A., Fedorov, E., Almo, S.C., Shoichet, B.K., and Raushel, F.M. (2007). Structure-based activity prediction for an enzyme of unknown function. Nature *448*, 775–779.

Hewitt, L., Kasche, V., Lummer, K., Lewis, R.J., Murshudov, G.N., Verma, C.S., Dodson, G.G., and Wilson, K.S. (2000). Structure of a slow processing precursor penicillin acylase from *Escherichia coli* reveals the linker peptide blocking the active-site cleft. J. Mol. Biol. *302*, 887–898.

Holm, L., and Sander, C. (1995). Dali: a network tool for protein structure comparison. Trends Biochem. Sci. *20*, 478–480.

Kabsch, W. (1993). Automatic processing of rotation diffraction data from crystals of initially unknown symmetry and cell constants. J. Appl. Crystallogr. *26*, 795–800.

Kim, Y., and Hol, W.G.J. (2001). Structure of cephalosporin acylase in complex with glutaryl-7-aminocephalosporanic acid and glutarate: insight into the basis of its substrate specificity. Chem. Biol. *8*, 1253–1264.

Kim, Y., Yoon, K., Khang, Y., Turley, S., and Hol, W.G.J. (2000). The 2.0 A crystal structure of cephalosporin acylase. Structure *8*, 1059–1068.

Kim, Y., Kim, S., Earnest, T.N., and Hol, W.G.J. (2002). Precursor structure of cephalosporin acylase. Insights into autoproteolytic activation in a new N-terminal hydrolase family. J. Biol. Chem. *277*, 2823–2829.

Lakomek, K., Dickmanns, A., Kettwig, M., Urlaub, H., Ficner, R., and Lübke, T. (2009). Initial insight into the function of the lysosomal 66.3 kDa protein from mouse by means of X-ray crystallography. BMC Struct. Biol. *9*, 56.

Luengo, J.M. (1995). Enzymatic synthesis of hydrophobic penicillins. J. Antibiot. (Tokyo) *48*, 1195–1212.

McVey, C.E., Walsh, M.A., Dodson, G.G., Wilson, K.S., and Brannigan, J.A. (2001). Crystal structures of penicillin acylase enzyme-substrate complexes: structural insights into the catalytic mechanism. J. Mol. Biol. *313*, 139–150.

Morris, R.J., Perrakis, A., and Lamzin, V.S. (2003). ARP/wARP and automatic interpretation of protein electron density maps. Methods Enzymol. *374*, 229–244.

Müller, W.H., Bovenberg, R.A., Groothuis, M.H., Kattevilder, F., Smaal, E.B., Van der Voort, L.H., and Verkleij, A.J. (1992). Involvement of microbodies in penicillin biosynthesis. Biochim. Biophys. Acta *1116*, 210–213.

Murshudov, G.N., Vagin, A.A., and Dodson, E.J. (1997). Refinement of macromolecular structures by the maximum-likelihood method. Acta Crystallogr. D Biol. Crystallogr. *53*, 240–255.

Murzin, A.G. (1996). Structural classification of proteins: new superfamilies. Curr. Opin. Struct. Biol. *6*, 386–394.

Murzin, A.G., Brenner, S.E., Hubbard, T., and Chothia, C. (1995). SCOP: a structural classification of proteins database for the investigation of sequences and structures. J. Mol. Biol. *247*, 536–540.

Noren, C.J., Wang, J., and Perler, F.B. (2000). Dissecting the chemistry of protein splicing and its applications. Angew. Chem. Int. Ed. Engl. *39*, 450–466.

Oinonen, C., and Rouvinen, J. (2000). Structural comparison of Ntn-hydrolases. Protein Sci. *9*, 2329–2337.

Otwinowski, Z., and Minor, W. (1997). Processing of X-ray diffraction data collected in oscillation mode. Methods Enzymol. *276*, 307–326.

Paulus, H. (2000). Protein splicing and related forms of protein autoprocessing. Annu. Rev. Biochem. *69*, 447–496.

Schneider, T.R., and Sheldrick, G.M. (2002). Substructure solution with SHELXD. Acta Crystallogr. D Biol. Crystallogr. *58*, 1772–1779.

Tobin, M.B., Fleming, M.D., Skatrud, P.L., and Miller, J.R. (1990). Molecular characterization of the acyl-coenzyme A:isopenicillin N acyltransferase gene (penDE) from *Penicillium chrysogenum* and *Aspergillus nidulans* and activity of recombinant enzyme in *Escherichia coli*. J. Bacteriol. *172*, 5908–5914.

Tobin, M.B., Cole, S.C., Kovacevic, S., Miller, J.R., Baldwin, J.E., and Sutherland, J.D. (1994). Acyl-coenzyme A: isopenicillin N acyltransferase from *Penicillium chrysogenum*: effect of amino acid substitutions at Ser227, Ser230 and Ser309 on proenzyme cleavage and activity. FEMS Microbiol. Lett. *121*, 39–46.

Tobin, M.B., Cole, S.C., Miller, J.R., Baldwin, J.E., and Sutherland, J.D. (1995). Amino-acid substitutions in the cleavage site of acyl-coenzyme A:isopenicillin N acyltransferase from *Penicillium chrysogenum*: effect on proenzyme cleavage and activity. Gene *162*, 29–35.

Vagin, A., and Teplyakov, A. (1997). MOLREP: an automated program for molecular replacement. J. Appl. Crystallogr. *30*, 1022–1025.

Whiteman, P.A., Abraham, E.P., Baldwin, J.E., Fleming, M.D., Schofield, C.J., Sutherland, J.D., and Willis, A.C. (1990). Acyl coenzyme A: 6-aminopenicillanic acid acyltransferase from *Penicillium chrysogenum* and *Aspergillus nidulans*. FEBS Lett. *262*, 342–344.

Winn, M.D., Murshudov, G.N., and Papiz, M.Z. (2003). Macromolecular TLS refinement in REFMAC at moderate resolutions. Methods Enzymol. *374*, 300–321.

Xu, Q., Buckley, D., Guan, C., and Guo, H.C. (1999). Structural insights into the mechanism of intramolecular proteolysis. Cell *98*, 651–661.

Yoshida, H., Hensgens, C.M.H., van der Laan, J.M., Sutherland, J.D., Hart, D.J., and Dijkstra, B.W. (2005). An approach to prevent aggregation during the purification and crystallization of wild type acyl coenzyme A: isopenicillin N acyltransferase from *Penicillium chrysogenum*. Protein Expr. Purif. *41*, 61–67.